journal

J. Am. Ceram. Soc., 79 [7] 1793–800 (1996)

Grain Growth in CeO_2: Dopant Effects, Defect Mechanism, and Solute Drag

Pei-Lin Chen* and I-Wei Chen*

Department of Materials Sciences and Engineering, University of Michigan, Ann Arbor, Michigan 48109-2136

The effects of the dopants, Mg^{2+}, Ca^{2+}, Sr^{2+}, Sc^{3+}, Yb^{3+}, Y^{3+}, Gd^{3+}, La^{3+}, Ti^{4+}, Zr^{4+}, and Nb^{5+}, on the grain boundary mobility of dense CeO_2 have been investigated from 1270° to 1420°C. Parabolic grain growth has been observed in all instances. Together with atmospheric effects, the results support the mechanism of cation interstitial transport being the rate-limiting step. A strong solute drag effect has been demonstrated for diffusion-enhancing dopants such as Mg^{2+} and Ca^{2+}, which, at high concentrations, can nevertheless suppress grain boundary mobility. Severely undersized dopants (Mg, Sc, Ti, and Nb) have a tendency to markedly enhance grain boundary mobility, probably due to the large distortion of the surrounding lattice that apparently facilitates defect migration. Overall, the most effective grain growth inhibitor at 1.0% doping is Y^{3+}, while the most potent grain growth promoter is either Mg^{2+} (e.g., 0.1%) or Sc^{3+} at high concentration (greater than 1.0%).

I. Introduction

GRAIN BOUNDARY mobility can be influenced by dopants in two distinct ways. First, grain boundary diffusivity of host ions is altered through defect chemistry and dopant–defect interactions. This may result in different populations or migration dynamics for the rate-controlling defect species. Alternatively, solute ions segregate to the grain boundary. This may result in a solute drag, so that grain boundary mobility is controlled by the lattice diffusion of the solute. These dopant effects on grain boundary mobility have long been recognized as important as they affect sinterability, microstructural stability, and creep. Nevertheless, systematic experimental documentation of these aspects in ceramics is still lacking. Recently, we have studied grain boundary mobility in CeO_2 containing trivalent dopants.[1] The present work completes this effort by extending it to similar systems containing divalent, tetravalent, and pentavalent dopants. In the accompanying paper, we also report a parallel study of Y_2O_3.[2]

CeO_2 is a prototypical fluorite-structured oxide. Like other oxides with this structure, it can easily incorporate many aliovalent cations by creating charge-compensating defects on the oxygen sublattice, V_O in the case of acceptor dopants[3–5] and O_i in the case of donor dopants.[6] In principle, oxides of this type, with cubic symmetry and with large cation solubilities, are relatively immune to abnormal grain growth caused by mobility disparity among different boundaries. Furthermore, since V_O forms very readily in this structure,[7–9] oxygen diffusion is very fast in CeO_2 and similar oxides, and invariably, cations are the rate-limiting species in the system. This makes CeO_2, which has no phase transformation (unlike ZrO_2) and is not radioactive (unlike UO_2, ThO_2, and PuO_2), a suitable model system for studying dopant effects on grain boundary mobility. In the present series of studies, we have investigated, in the order of increasing charge/size, the following dopants: Mg^{2+}, Ca^{2+}, Sr^{2+}, Sc^{3+}, Yb^{3+}, Y^{3+}, Gd^{3+}, La^{3+}, Ti^{4+}, Zr^{4+}, and Nb^{5+}.

An interesting aspect of CeO_2 is the special chemistry of Ce^{4+}, which can readily reduce itself to Ce^{3+}. This property is the basis of several technological applications of CeO_2, such as catalytic supports (for automotive exhaust) and high-temperature electrodes. In the present context, it also dictates that a large population of charge-compensating V_O already exists in undoped CeO_2. Therefore, for dopant studies, it is necessary to distinguish an intrinsic regime, in which V_O population is largely tied to Ce^{3+}, from an extrinsic regime, in which V_O is mainly affected by aliovalent dopants. Calculations presented in our previous work,[1] replotted in Fig. 1, indicate that the concentration of Ce^{3+} is between 0.2% to 0.8% in the temperature range of 1270° to 1420°C. By adjusting the dopant concentration to lie above or below this band, either an extrinsic or intrinsic regime can be accessed for comparative studies. This strategy has been followed in our work. In the previous investigation on trivalent dopants, we also found that the dopant effect on grain boundary mobility was primarily through defect–dopant interactions in the intrinsic regime, and through solute drag in the extrinsic regime. This distinction is further investigated in the present work using other dopants.

In principle, grain growth experiments offer an opportunity to investigate the diffusion mechanisms of pure and doped systems. Although this probe to diffusion is indirect and sometimes complicated by the simultaneous operation of grain boundary and lattice (solute drag) mechanisms, it has the advantage of involving only a relatively short diffusion distance

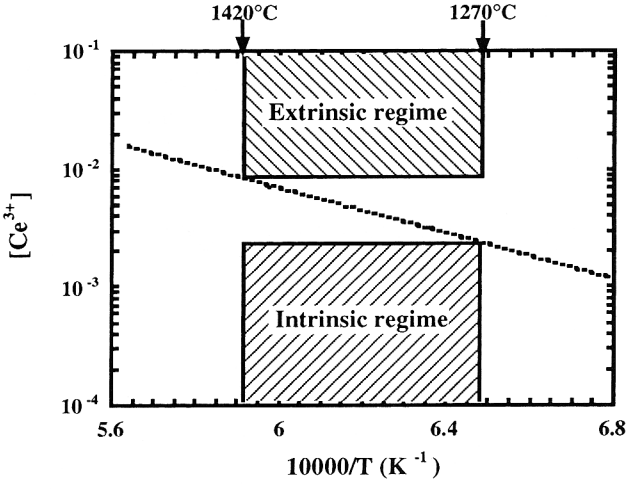

Fig. 1. Defect concentration, $[Ce^{3+}]$, vs reciprocal temperature for undoped CeO_2 in air (data from Ref. 6). Intrinsic and extrinsic regimes for dopant concentrations shown between 1270° and 1420°C.

C. A. Handwerker—contributing editor

Manuscript No. 192270. Received October 9, 1995; approved February 1, 1995.
Presented at the 95th Annual Meeting of the American Ceramic Society, Cincinnati, OH, April 21, 1993 (Sintering and Microstructure Development Symposium, Paper No. SXV-36-93).
Supported by the U.S. Department of Energy under Grant No. DE-FG02-87ER45302.
*Member, American Ceramic Society.

(several tens of micrometers) and very good sampling statistics (several hundred grains). These advantages allow grain growth experiments to be performed at relatively low temperatures, compared to conventional diffusion ones, and to provide valuable insight to the diffusion mechanisms. Analyzing grain growth data in our previous study on CeO_2, we found that cations diffuse by an interstitial mechanism.[1] This finding has been further substantiated in the present work using other dopants, and we now believe that it is general for all fluorite-structured sub-oxides such as UO_{2-x} and $(U,Pu)O_{2-x}$.[10] Lastly, we have again observed some anomalous effects of severely undersized dopants on lattice distortion, defect interaction, and migration which were first reported for Sc in our previous publication.[1] Further evidence for these effects and their structural origins are presented in the following.

II. Experimental Procedure

Ultrafine highly reactive CeO_2 powders prepared by a homogeneous precipitation method as described in our previous paper[11] were used as starting powders. The CeO_2 powders were first dispersed in isopropyl alcohol to which dopants were added in the form of nitrates. The doped powders were then calcined to effect homogenization. As in our previous work on trivalent dopants,[1] dopant concentrations were fixed at 0.1% or 1.0% of the total cations, except for Nb^{5+}, for which the lower solubility in CeO_2 limited the maximum Nb^{5+} concentration to 0.6%. The ionic size[12] and solubility[6,13–17] of these dopants are listed in Table I. To avoid SiO_2 contamination, powder processing was conducted using plastic ware only, and sintering and experiments of grain growth, mostly in air, were performed using a dedicated "clean" furnace. High-purity flowing O_2 was also used in some experiments to provide a controlled atmosphere for comparison. This and other procedures are identical to those described in our previous work on CeO_2 with trivalent dopants.[1]

The microstructures of the sintered specimens were characterized by a scanning electron microscope (SEM) after polishing and thermal etching. The grain size was obtained by multiplying the average linear intercept length of at least 500 grains by 1.56.[18] In addition, the average grain diameter for each grain was used to evaluate the grain size distribution. For grain growth study, only samples with a density higher than 99% were used to avoid the influence of porosity on grain boundary mobility.

III. Results

(1) Microstructures

Selected microstructures are displayed in Fig. 2 to demonstrate the difference in grain size. A representative microstructure of undoped CeO_2 (sintered in air at 1270°C for 1.2 h) is shown in Fig. 2(a). Among all the samples with divalent cation dopants, over the range of temperature studied, the smallest grain size observed in the fully dense samples was 0.68 μm, as in the case of 1% Ca doping sintered at 1270°C for 1.2 h shown in Fig. 2(b). The largest grain size was 31 μm, as in the case of 0.1% Mg doping sintered at 1420°C for 6 h shown in Fig. 2(c). With tetravalent cation doping, the smallest grain size obtained was 0.59 μm as in the case of 1% Zr doping sintered at 1270°C for 1.2 h shown in Fig. 2(d), and the largest grain size was 34.6 μm as in the case of 0.1% Ti doping sintered at 1420°C for 6 h as shown in Fig. 2(e). Nb-doped samples had a grain size in between the above extremes and are not shown here.

Table I. Ionic Radius and Solubility of MO_x in CeO_2

	Ionic radius† (Å)	Solubility (%$MO_{1.5}$)	Ref.
Mg^{2+}	0.89	2 (1600°C)	13
Ca^{2+}	1.12	9 (1600°C)	14
Sr^{2+}	1.26	9 (1600°C)	14
Sc^{3+}	0.87	9.5 (1750°C)	13, 15
Yb^{3+}	0.99	40 (1400°C)	15, 16
Y^{3+}	1.02	48.6 (1400°C)	13, 15, 16
Gd^{3+}	1.053	100 (1400°C)	15, 16
La^{3+}	1.16	45 (1600°C)	15, 16
Ti^{4+}	0.74		
Zr^{4+}	0.84	30 (1400°C)	15
Ce^{4+}	0.97		
Nb^{5+}	0.74	0.6 (1320°C)	6

†Reference 12. All for 8-fold coordination.

(2) Grain Size Measurement

As evident in Fig. 2, no abnormal grain growth has taken place in all the cases studied. To ascertain this point, grain size distributions were measured for selected compositions and the results are shown in Fig. 3 in the form of normalized grain size. It was found that despite the large difference in mean grain size (from 2.5 to 18 μm), the majority of grains had a size centered around the mean and there was no abnormal growth as evidenced by the absence of a second peak at larger sizes. This allowed us to use the average linear intercept length to represent the grain size and to evaluate growth kinetics.

Following our previous paper,[1] we found the mobility data agree with the parabolic law well:

$$d^2 - d_0^2 = 2M\gamma(t - t_0) \tag{1}$$

where d_0 is the reference grain size at time t_0, d is the average grain size at time t, γ is grain boundary energy, and M is the mobility of grain boundary. This equation follows directly from the equation of motion of grain size and is strictly valid provided M and γ are time (size) independent:[19]

$$\frac{\delta d}{\delta t} = M\gamma/d \tag{2}$$

To avoid the influence of porosity on grain boundary mobility, the time t_0 was chosen so that the sintered density had at least achieved 99%. Typical values of t_0 are 1.2 h at 1270°C and 6 min at 1420°C. Then, by plotting $d^2 - d_0^2$ against $t - t_0$, we could identify and obtain a straight-line fit that passes through the origin with a slope representing the average $2M\gamma$. Some of the grain size data, for samples sintered at 1270°C, are plotted in Fig. 4 to illustrate this procedure and the excellent fit. Since it is obvious that the value of the slope varies over many orders of magnitude, and since this large variation is not likely due to γ, which typically varies by no more than a factor of 2 over a wide range of temperature and composition, we have assumed as in our previous paper[1] γ to remain constant, taken to be 0.3 J/m^2, for the purpose of evaluating the grain boundary mobility. The mobility data obtained in this way are summarized in Table II which, for completeness, also includes our previous data for trivalent dopants. These data are analyzed below to infer diffusion and grain growth mechanisms.

IV. Diffusion Mechanism for Cations

The mobility data at low dopant concentrations can be used to deduce the diffusion mechanism for host cations. At this point, we do not distinguish grain boundary diffusion from lattice diffusion, but concentrate instead on the implications of defect chemistry which should be applicable to both cases. In the dilute concentration range, we expect Ce diffusion to be rate limiting. (There is no need to distinguish diffusitivies of Ce^{3+} and Ce^{4+} cations, since they interchange by exchanging charge via the small polaron mechanism which has an activation energy much smaller than that of cation diffusion.[20]) From the defect reactions

Schottky defect formation:

$$\text{null} \xleftrightarrow{\Delta G_S} V_{Ce}'''' + 2V_O^{\cdot\cdot} \tag{3}$$

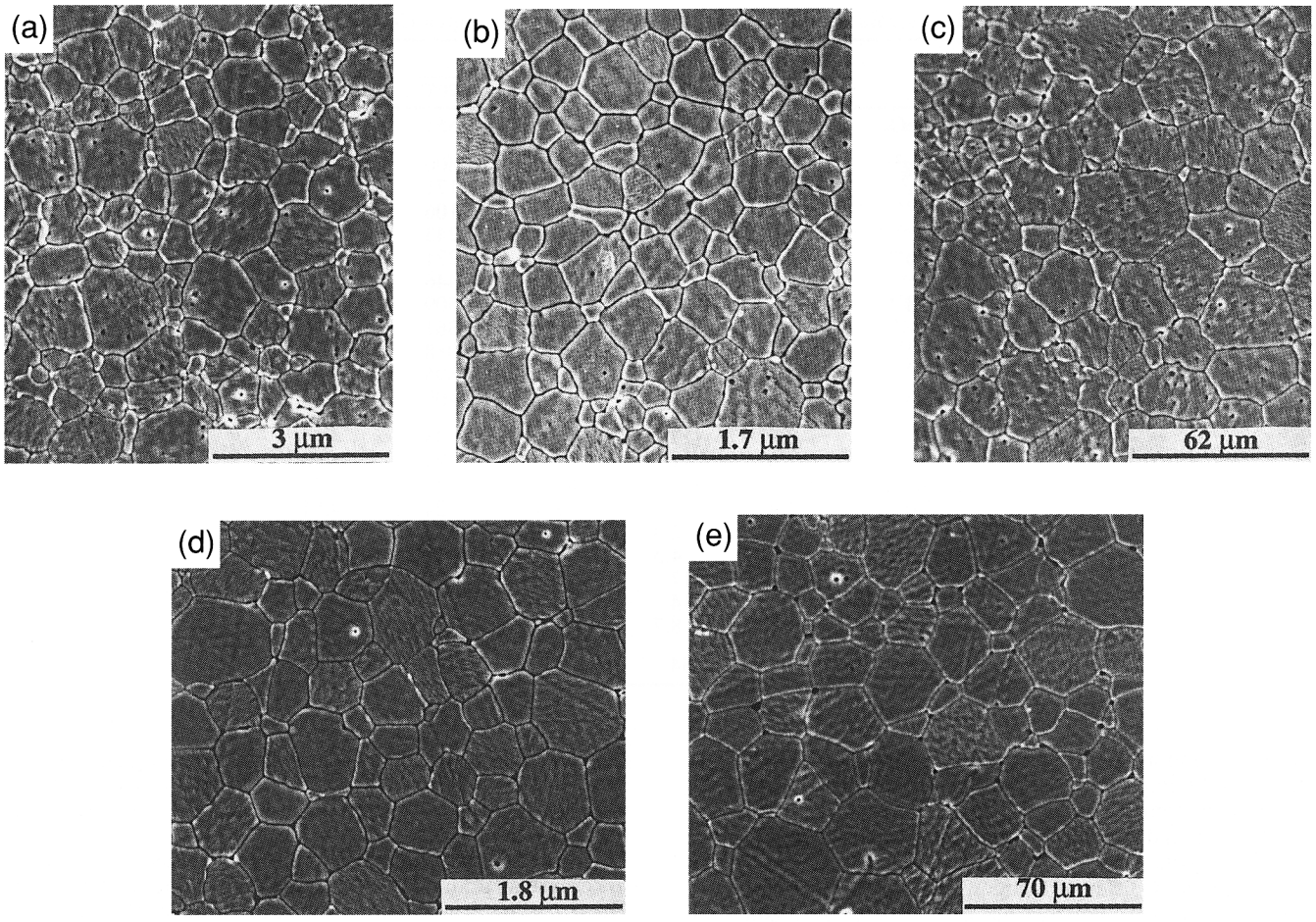

Fig. 2. Microstructures of undoped and doped CeO_2: (a) CeO_2 (1270°C/1.2 h); (b) 1.0% Ca (1270°C/1.2 h); (c) 0.1% Mg (1420°C/6 h); (d) 1.0% Zr (1270°C/1.2 h); (e) 0.1% Ti (1420°C/6 h).

Frenkel defect formation:

$$\text{null} \xleftrightarrow{\Delta G_F} V_{Ce}'''' + Ce_i^{\cdots} \tag{4}$$

we find

$$[V_{Ce}''''] = [V_O^{\cdot\cdot}]^{-2} \frac{K_F}{K_S} \exp\left(-\frac{\Delta G_F}{kT}\right) \tag{5}$$

$$[Ce_i^{\cdots}] = [V_O^{\cdot\cdot}]^{2} \frac{K_F}{K_S} \exp\left(-\frac{\Delta G_F - \Delta G_S}{kT}\right) \tag{6}$$

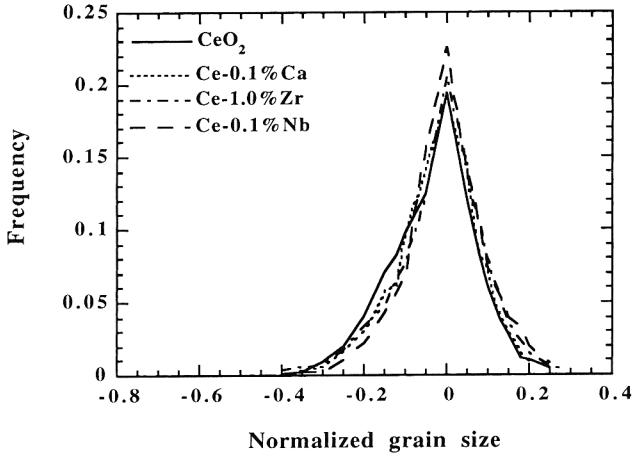

Fig. 3. Grain size distributions of undoped and doped CeO_2. Grain size is normalized by mean grain size in each case, which varies from 2.5 to 18 μm.

In the above, K_F and K_S are the preexponential, temperature-independent, factors of the reaction constants of Eqs. (3) and (4), respectively. At equilibrium, Eqs. (5) and (6) are applicable to both the bulk and grain boundaries. Since cation diffusion is rate-limiting and is by either an interstitial or a vacancy mechanism, the concentrations of these defects have a direct bearing on the cation diffusivity and hence the grain boundary mobility. Therefore, by examination of the dependence of the grain boundary mobility on oxygen vacancy concentrations, the diffusion mechanism can be ascertained.

Previously, we have noted that the grain boundary mobility in undoped CeO_2 is higher in a less oxidizing atmosphere (e.g.,

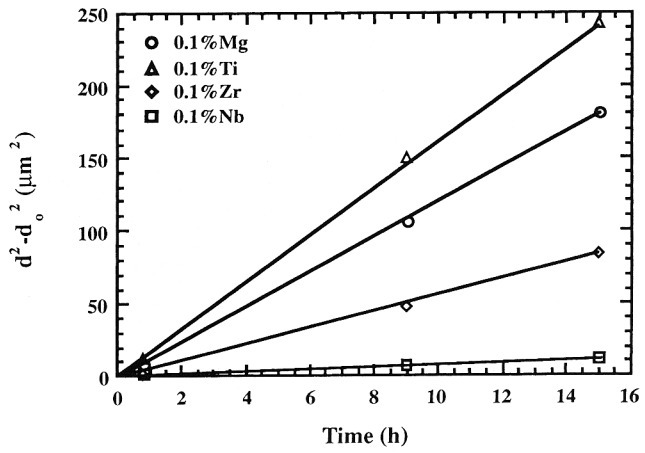

Fig. 4. Grain growth kinetics of CeO_2 at 1270°C. Dopants as indicated.

Table II. Grain Boundary Mobility of Undoped and Doped CeO_2 in Air

		Mobility ($\times 10^{-16}$ m^3/(N·s))				Activation energy (eV)
		1270°C	1320°C	1370°C	1420°C	
	CeO_2	10	36	169	551	6.16
0.1%	Mg^{2+}	70	250	700	1800	4.86
	Ca^{2+}	41	150	430	1171	5.02
	Sr^{2+}	29	110	330	1106	5.42
	Sc^{3+}	3.3	12	62	243	7.01
	Yb^{3+}	3.6	17	70	271	6.48
	Y^{3+}	27	72	229	446	4.88
	Gd^{3+}	33	100	247	509	3.79
	La^{3+}	9.3	26	136	361	6.19
	Ti^{4+}	48	140	365	1018	4.55
	Zr^{4+}	11	42	180	595	6.05
	Nb^{5+}	8	31	142	400	5.98
1.0%	Mg^{2+}	8.8	27.1	71	193	4.61
	Ca^{2+}	3.6	11	27	75	4.50
	Sc^{3+}	206	461	664	1045	2.37
	Yb^{3+}	1.4	3.1	12	24	4.51
	Y^{3+}	0.7	2.3	7.8	18	4.94
	Gd^{3+}	1.7	4.5	12	38	4.66
	La^{3+}	4.7	17	49	101	4.73
	Ti^{4+}	4.2	14	37	97	4.70
	Zr^{4+}	2.2	8.7	25	63	5.02
0.6%	Nb^{5+}	14	34	121	350	4.89

2% O_2) than in a more oxidizing atmosphere (e.g., 100% O_2). These results imply enhanced diffusion with increasing $[V_O^{\cdot\cdot}]$ and are consistent with Eq. (6). Since $[V_O^{\cdot\cdot}]$ can also be influenced by cation dopants, this aspect is examined first.

Figure 5 plots some of the mobility data of CeO_2 in air with 0.1% dopants of different charges. For each charge state, the dopant chosen is the one that has the smallest size misfit with the host Ce^{4+}. When possible, the undersized dopants are also excluded since they tend to have very strong interactions with the defects and have anomalous effects on defect migration (see Section VI). As seen in Fig. 5, a trend of decreasing mobility in the same atmosphere is seen with dopants of increasing valence which are marked by arrows on the right. Since acceptors such as Ca^{2+} and Y^{3+} are expected to increase $[V_O^{\cdot\cdot}]$, and donors such as Nb^{5+} are expected to decrease $[V_O^{\cdot\cdot}]$, this trend is again consistent with the interstitial mechanism only. Indeed, Zr^{4+}, which does not affect $[V_O^{\cdot\cdot}]$, has little effect on the mobility. The atmospheric effect is also shown in Fig. 5 and is consistent with the interstitial mechanism only: a more oxidizing atmosphere, such as flowing O_2, decreases $[V_O^{\cdot\cdot}]$ and likewise suppresses the mobility. This is confirmed for Nb-doped CeO_2 just as for undoped CeO_2 before.

The interstitial mechanism can be rationalized by inspecting the crystal structure of CeO_2. In the fluorite structure shown in Fig. 6, cations occupy only one half of the cube interstitial sites which are surrounded by eight oxygen ions. Cation diffusion will most likely pass through these unoccupied interstitial sites, since they are vacant and the passage through the saddle point S_A is relatively open. (Direct hopping between two adjacent cations sites, even when one is empty, probably is more difficult because of the narrower passage at the saddle point, S_B.) Evidence for interstitial diffusion in fluorite-structured oxides was previously reported for UO_{2-x}[10] and $(U,Pu)O_{2-x}$.[21] In addition, cubic Bi_2O_3[22] and Y_2O_3,[2] which have a so-called C-type rare-earth oxide structure that is very similar to the fluorite structure, seem to favor an interstitial mechanism for cation diffusion as well. Lastly, cubic ZrO_2 which has a much higher $[V_O^{\cdot\cdot}]$ than tetragonal ZrO_2, is also known to have a much higher grain boundary mobility than the latter.[23] This leads us to believe that the cation interstitial mechanism is an intrinsic feature of this class of oxides, whenever oxygen vacancies predominate.

The grain boundary mobility of CeO_2 in the intrinsic regime should follow

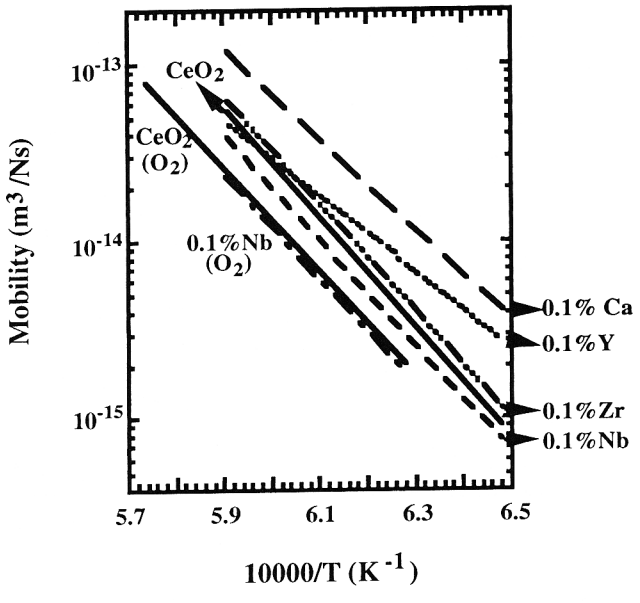

Fig. 5. Grain boundary mobility of undoped and 0.1%-doped CeO_2.

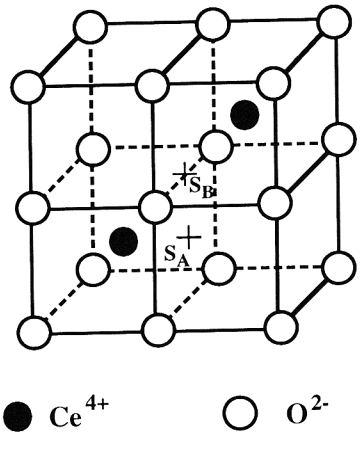

Fig. 6. Unit cell of the fluorite crystal structure.

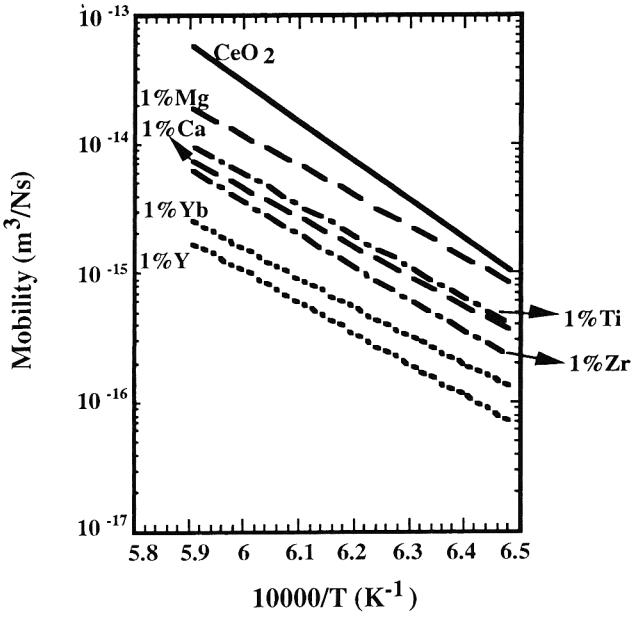

Fig. 7. Grain boundary mobility of undoped and 1.0%-doped CeO_2.

$$M_{\text{intrinsic}} \propto \mathcal{D}^{\text{gb}}_{\text{Ce}_i}[V_O^{\cdot\cdot}]^2 \frac{K_F}{K_S} \exp\left[-\frac{\Delta G_F - \Delta G_S}{kT}\right] \tag{7}$$

where $\mathcal{D}^{\text{gb}}_{\text{Ce}_i}$ is the self-diffusivity of Ce_i along a grain boundary. For pure CeO_2, $[V_O^{\cdot\cdot}]$ is determined by redox reaction between Ce^{4+} and Ce^{3+}

$$O_2 + 4Ce'_{Ce} + 2V_O^{\cdot\cdot} \overset{\Delta H_{O_2}}{\longleftrightarrow} 4Ce_{Ce} + 2O_O \tag{8}$$

which gives

$$[V_O^{\cdot\cdot}] = K'_{O_2} \exp\left(\frac{-\Delta H_{O_2}}{6kT}\right) \tag{9}$$

(Note that K'_{O_2}, the reaction constant, has an implicit dependence on the partial pressure of O_2 varying as $P_{O_2}^{-1/6}$.) For undoped CeO_2, $\Delta H_{O_2} \sim 9$ eV from Ref. 24, and the activation energy of grain boundary mobility is ~6 eV. If we adopt the same defect energy $\Delta G_S \sim 6.4$ eV and $\Delta G_F \sim 9.5$ eV for CeO_2 as for UO_2,[25] in view of the similar cation size and charge, we conclude that the activation energy in $\mathcal{D}^{\text{gb}}_{\text{Ce}_i}$ is relatively small, 0.1 eV or nearly zero. Despite such a small activation energy for interstitial diffusion, the activation energy of grain boundary mobility in undoped CeO_2 is relatively high because of the temperature dependence of $[V_O^{\cdot\cdot}]$. This is responsible for the steeper slope of the data of undoped CeO_2 in Fig. 5 compared with other data.

V. Solute Drag in the Extrinsic Regime

At 1.0% doping, grain boundary mobility of doped CeO_2 in most cases is lower than that of undoped CeO_2. This not only applies to Zr^{4+} doping, which should have little effect on defect concentration, but also to acceptor doping, which should enhance diffusivity by increasing oxygen vacancies. Mobility data of Mg^{2+}, Ca^{2+}, Y^{3+}, Yb^{3+}, Ti^{4+}, and Zr^{4+} doping are shown in Fig. 7 along with those of undoped CeO_2 to demonstrate this point. The suppression of mobility in this case can be attributed to solute drag which is expected to increase with reciprocal lattice diffusivity of the solute. Since both elastic (due to size and modulus misfit) and electrostatic (due to charge mismatch) interactions between solutes and the grain boundary can be responsible for the buildup of the solute cloud, aliovalent and isovalent dopants alike can participate in this mechanism. The drag is also expected to increase with the solute content. This is consistent with the observation that only at 1.0% doping, but not 0.1% doping, was the drag effect evident.

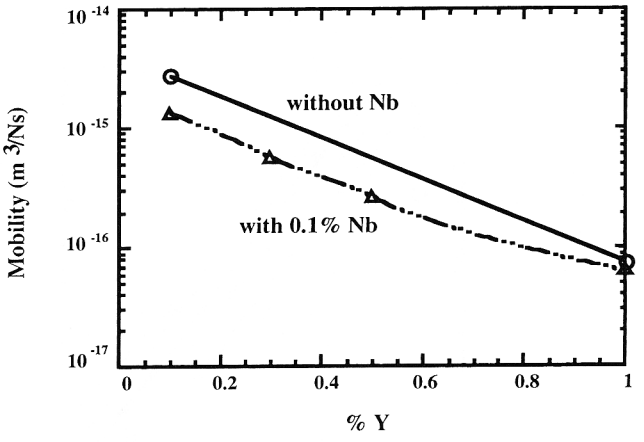

Fig. 8. Grain boundary mobility of Y-doped and Y/Nb-doped CeO_2 at 1270°C.

At 1.0%, acceptor dopants are expected to dominate the defect concentration. Thus, $[V_O^{\cdot\cdot}]$ should be temperature independent, and the temperature dependence of $[Ce_i^{\cdot\cdot\cdot\cdot}]$ is determined by $\Delta G_F - \Delta G_S$. Assuming diffusion of acceptor cations follows the same interstitial mechanism, they should incorporate the same temperature dependence as $[Ce_i^{\cdot\cdot\cdot\cdot}]$. It then follows that the grain boundary mobility in the solute drag regime

$$M_{\text{solute drag}} \propto \mathcal{D}^{\text{lattice}}_{\text{D}_i}[V_O^{\cdot\cdot}]^2 \frac{K_F}{K_S} \exp\left[-\frac{\Delta G_F - \Delta G_S}{kT}\right] \tag{10}$$

The mobility data in Table II indicate that for Mg^{2+}, Ca^{2+}, Yb^{3+}, Y^{3+}, Gd^{3+}, and La^{3+} the activation energies all lie between 4.5 and 5.0 eV. This value is the sum of $\Delta G_F - \Delta G_S$ and $\Delta H^{\text{lattice}}_{\text{D}_i}$, the latter being the migration energy of (dopant) cation interstitial in the bulk. Adopting the same value for $\Delta G_F - \Delta G_S \sim 3.0$ eV, we conclude that $\Delta H^{\text{lattice}}_{\text{D}_i}$ is around 1.5 to 2.0 eV for most dopants of a comparable size as Ce^{4+}.

The relative magnitude of the grain boundary mobilities with different dopants does not follow a simple trend, although smaller dopants in each isoelectrical group tend to correspond to higher mobilities. This is not surprising since the mobility, when controlled by solute drag, depends not only on Eq. (10) but also on the solute–grain boundary interaction. While CeO_2 doped with cations of different charges should see its diffusivity decrease with increasing charge of the dopants, the electrostatic interaction between dopants and grain boundary also decreases from divalent to trivalent dopants and vanishes for tetravalent dopants, possibly resulting in less segregation and a smaller drag. Apparently, these two opposing trends are in competition in Fig. 7 causing the mobility to first decrease from $(Mg,Ca)^{2+}$ to $(Yb,Y)^{3+}$ (due to fewer $V_O^{\cdot\cdot}$), then increase to $(Ti,Zr)^{4+}$ (due to less interaction).

Nb doping is expected to lower $[V_O^{\cdot\cdot}]$ and hence depress diffusivity according to the cation interstitial mechanism, if $V_O^{\cdot\cdot}$ dominates the defect population. For CeO_2 doped with 0.1% Y (in the intrinsic regime) and 1.0% Y (in the extrinsic regime), as well as intermediate concentrations in between, additional Nb doping at 0.1% always suppresses the mobility as shown in Fig. 8. Thus, the interstitial mechanism appears to persist throughout both regimes, which, for grain boundary mobility, encompass grain boundary and lattice diffusion.

VI. Undersized Dopants

Severely undersized dopants such as Nb^{5+}, Ti^{4+}, Sc^{3+}, and Mg^{2+} have an anomalous effect on grain boundary mobility. This is illustrated in Fig. 9 for Nb^{5+}, which suppresses mobility at low concentration, 0.1%, but the trend is partially reversed at

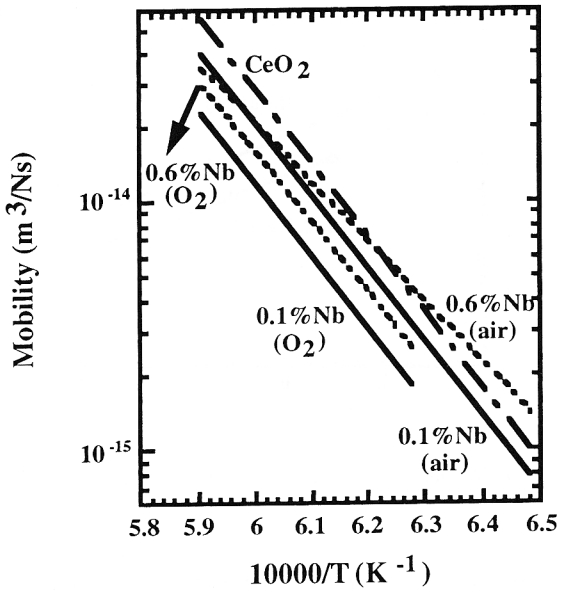

Fig. 9. Grain boundary mobility of Nb-doped CeO_2.

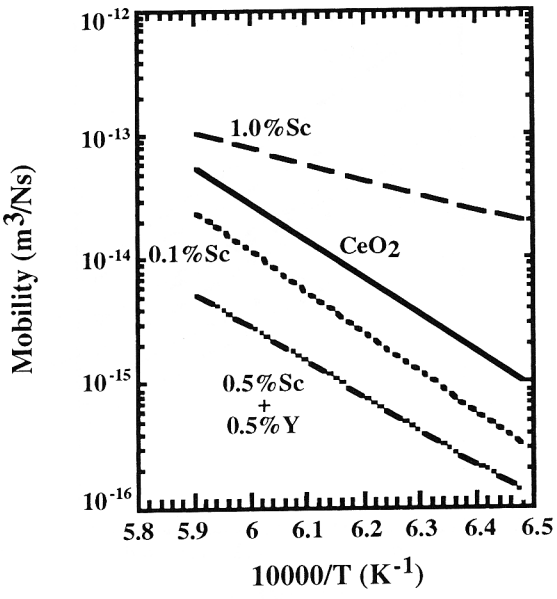

Fig. 10. Grain boundary mobility of undoped and doped CeO_2.

high concentration, 0.6%. Since Nb^{5+} is expected to lower the concentration of cation vacancies, and such an effect is indeed verified by comparing the mobility data in air (higher) and in O_2 (lower), the anomalous effect cannot be due to a change of defect mechanism. Instead, we found that this effect is associated with a tendency for undersized dopants to enhance diffusion. This effect is seen for other severely undersized dopants as well; for example, at 1.0% Mg doping yields a higher mobility than Ca doping, as does Ti doping a higher mobility than Zr doping. These data belong to the solute drag regime and were already shown in Fig. 7. At 1.0% Sc doping, the enhancement effect is so large that it totally negates the solute drag resulting in a mobility much higher than that of undoped CeO_2 at all temperatures. This is shown in Fig. 10 along with other data for relevant comparisons. These include the data of 0.1% Sc and 0.5% Sc + 0.5% Y, which show another anomalous effect of suppressing grain boundary mobility, also because of the size effect but for a different reason, as will become clear in the next section.

To understand these results, we first note that, at 1.0%, the dopants are already fairly closely spaced. This should be apparent if we simply recall that in a cubic lattice, the spacing between dopants of 1% concentration is only five cations apart, on average. Thus, dopants can exert a large effect on each other and on defect diffusion through lattice distortion and electrostatic interactions. Since the anomalous effect seems to be independent of the dopant charge, and is only observed for undersized dopants, certain asymmetry in lattice distortion that is exacerbated by undersized dopants is the most likely cause for it. Large lattice distortion around undersized dopant has been experimentally verified for Sc^{3+} in CeO_2,[26] and for Ga^{3+}, Fe^{3+}, and Nb^{5+} in ZrO_2,[27] using extended X-ray absorption fine structure (EXAFS). Unlike those of host cation or oversized dopant cations, the EXAFS spectra of undersized dopants lack a distinct Fourier-transform peak that corresponds to the nearest-neighbor cation–cation correlation that is otherwise most prominent for crystalline oxide EXAFS. This is because the cation–cation arrangements are so severely disturbed around these dopants that they completely suppress, by destructive interference of photoelectron waves, what would have corresponded to the cation–cation correlation in the nearest neighbor. Theoretically, we have suggested that the asymmetry of lattice distortion can be understood by the asymmetry around the minimum of interatomic potential. As shown in Fig. 11, when a solute atom with a size misfit occupies a regular lattice site, the distance (a_0) between lattice sites for cations does not coincide with the bond distance ($r_{equilibrium}$) at the potential minimum. Unlike an oversized solute that is pressed against its neighbors ($a_0 < r_{equilibrium}$) and is resisted by a very stiff repulsive potential, a severely undersized solute ($a_0 > r_{equilibrium}$) experiences a much softer potential. In particular, when the size of the solute is so small that a_0 exceeds the inflection point, r^*, shown in Fig. 11, the restoring force (which is the negative first derivative of the potential) actually decreases with further increase of cation–cation distance. If $a_0 > r^*$, any perturbation will lead to an off-centered displacement of the solute cation. This is believed to be the fundamental cause of the anomalous effect of undersized dopants. Large off-centered distortions of undersized dopants have indeed been observed in lattice simulation of defect structure using the Mott–Littleton model for ionic solids for both NaCl structure (Mg^{2+}, Mn^{2+}, Fe^{2+}, Co^{2+}, and Ni^{2+}, in CaO, SrO, and BaO)[28] and fluorite structure (Sc in CeO_2).[29]

Strong, attractive interaction between undersized dopants and $V_O^{\cdot\cdot}$, which does exist for Sc, is not likely to enhance diffusion, since such interaction ties up "free" $V_O^{\cdot\cdot}$ and has just the opposite effect (see next section). On the other hand, the large lattice disruption caused by severely undersized dopants can distort the saddle point configuration of the migrating defect. In this way, it is possible to effect an enhancement in the diffusivity of the host or dopant cation by lowering the migration enthalpy or increasing the preexponential factor (e.g., due to an increase of vibration entropy in the presence of a flat potential). This can explain their anomalous enhancement effect on grain boundary mobility. The other case of anomalous suppression effect on grain boundary mobility is discussed next.

VII. Dopant–Defect Association

Both electrostatic interaction and elastic interaction are present in ionic solids. The dopant–defect forces due to these interactions may be either additive or subtractive. It is therefore best, for simplicity, to inspect cases for which both elastic and electrostatic interactions are attractive for the dominant defect species. Since $V_O^{\cdot\cdot}$ is predominant in CeO_2, acceptor dopants with a large size mismatch have both the strongest elastic and the strongest electrostatic attractions with $V_O^{\cdot\cdot}$. To further avoid the anomalous effect of undersized dopants on saddle point configurations, we will first examine the case of 0.1% doping with oversized acceptors. We also assume that the concentration of "free" $V_O^{\cdot\cdot}$ not bound by the dopants is the one that enters

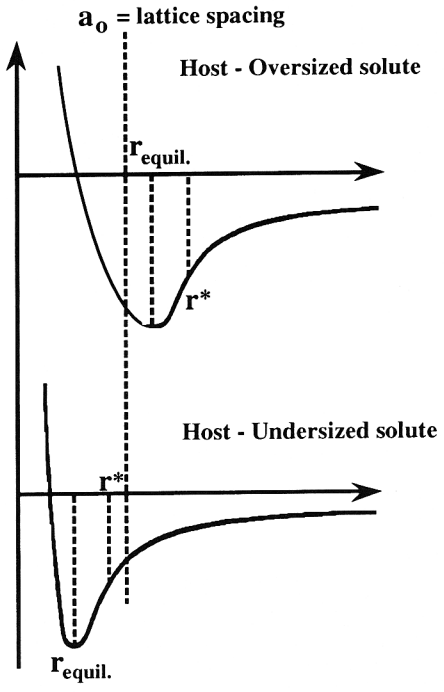

Fig. 11. Interatomic potential between a host cation and an oversized/undersized dopant. r^* is inflection point.

Eq. (6) to determine $[Ce_i'''']$, which directly controls cation diffusion.

Among divalent dopants, we expect Sr^{2+} to have a stronger attraction with $V_O^{\cdot\cdot}$ than Ca^{2+}, due to the larger size misfit. Thus, the concentration of "free" $V_O^{\cdot\cdot}$ should be lower in Sr^{2+}-doped CeO_2 and so should $[Ce_i'''']$. A lower grain boundary mobility in 0.1%-Sr^{2+}-doped CeO_2, compared to 0.1%-Ca^{2+}-doped CeO_2, was indeed observed. In addition, a higher activation energy by about 0.4 eV was found for Sr doping. This reflects the progressive dissociation of the dopant–$V_O^{\cdot\cdot}$ complexes at higher temperature, with the temperature dependence becoming steeper the larger the dissociation energy. A similar comparison can be made between La^{3+} and Y^{3+}, which reveals the same trend indicating a stronger attraction between the larger La^{3+} and $V_O^{\cdot\cdot}$.

We now return to the particular observation of mobility suppression by 0.1% Sc and 0.5% Sc + 0.5% Y shown in Fig. 10. In essence, this is the same "scavenging" effect first noted by Nowick and co-workers[4] in ionic conductivity of CeO_2 with trivalent dopants. It arises because, for trivalent dopants, only one $V_O^{\cdot\cdot}$ is generated for every two cation dopants. Thus, trivalent dopants that have a very strong attraction for $V_O^{\cdot\cdot}$ can "scavenge" the $V_O^{\cdot\cdot}$ created by other trivalent dopants. In particular, Sc doping can deplete the concentration of "free" $V_O^{\cdot\cdot}$ in the undoped CeO_2 in which the $V_O^{\cdot\cdot}$ is created by Ce^{3+}. Such a scavenging effect is seen for 0.1% Sc doping shown in Fig. 10. A very large activation energy, compared to that of doping with other dopants at the same concentration, is evident and again supports the notion of dopant–$V_O^{\cdot\cdot}$ association in this case. The scavenging effect of Sc doping can also be seen at higher concentration, if additional $V_O^{\cdot\cdot}$ are provided by other trivalent dopants, as in the case of 0.5% Sc + 0.5% Y doping also shown in Fig. 10. Here, each Sc^{3+} is believed to be associated with one $V_O^{\cdot\cdot}$ (generated by both Sc^{3+} and Y^{3+}), so once again very few "free" $V_O^{\cdot\cdot}$ are available to effect the cation interstitial defect mechanism of diffusion. Since no anomalous enhancement effect on grain boundary mobility was found in this case at all, we also believe that all the Sc^{3+} have been tied up in the form of complexes (Sc–V_O) which have no large lattice distortion beyond itself and will not disrupt the saddle point configurations of cation interstitials. This, in fact, was previously suggested by the EXAFS data[25] which found the very large distortion around Sc^{3+} in CeO_2 is much reduced once an equal amount of (oversized) Gd^{3+} dopants was additionally incorporated.

VIII. Discussion

While the basic trends of the intrinsic grain boundary mobility and the dopant effects have been outlined and a mechanistic interpretation based on defect chemistry and dopant–defect interaction have been proposed, the data have only been rationalized qualitatively at this point. (Some attempt to develop a trapping model based on Fermi–Dirac statistics has been made in our previous paper[1] for dilute doping, with moderate success.) A more quantitative analysis is presently hampered by the relative uncertainty of the magnitude of interaction energy, the anomalous effect of undersized dopants on migration entropy and enthalpy, and the lack of a more detailed knowledge of dopant concentration dependence. Nevertheless, our interpretation of the data is self-consistent and not in violation of the basic thermodynamic and kinetic principles. In the following, some additional comments or the possible complications of this interpretation and their resolution are made for completeness.

(1) Ti

Ti itself is a cation that has variable valences, Ti^{3+} and Ti^{4+}. Thus, some effect of Ti^{3+} on the formation of $V_O^{\cdot\cdot}$ is possible especially at small dopant concentration. This is probably the cause for the higher mobility in 0.1%-Ti^{4+}-doped CeO_2 compared to 0.1%-Zr^{4+}-doped CeO_2.

(2) Zr

At dilute concentration, Zr^{4+} has little effect on grain boundary mobility, and the activation energy is almost the same as that of undoped CeO_2. This is a confirmation of its charge-neutral status as a dopant. At 1% doping, we expect $[V_O^{\cdot\cdot}]$ is still intrinsically controlled (by Ce^{3+}) but that lattice diffusion is rate limiting (i.e., in the solute drag regime). Since activation energy of undoped CeO_2 is around 6.0 eV and the difference in migration energy in the lattice and in the grain boundary is estimated to be about 1.5 eV, we expect an activation energy of around 7.5 eV. The observed value 5.0 eV is lower than this estimate. Since Zr^{4+} is undersized, at high concentration, it probably also causes some anomalous enhancement effect similar to that of other severely undersized dopants. Note that a similar magnitude of activation energy difference, 2.5 eV, is also seen when comparing data of 1.0% Sc doping with 1.0% rare earth cation doping.

IX. Conclusions

(1) Grain boundary mobility in CeO_2 is controlled by cation diffusion, and cations diffuse by an interstitial mechanism that can be enhanced by the presence of oxygen vacancies.

(2) At high dopant concentrations (1.0% in this case), a solute drag mechanism operates that suppresses grain boundary mobility.

(3) Severely undersized dopants (Mg, Sc, Ti, and Nb) have a tendency to markedly enhance grain boundary mobility, probably due to the large distortion of the surrounding lattice that apparently facilitates defect migration.

(4) Grain boundary mobility is further influenced by dopant–defect interaction which is charge and size dependent. Overall, 0.1% Mg and 1.0% Sc increase the mobility the most, while 1.0% Y decreases the mobility the most.

References

[1]P.-L. Chen and I-W. Chen, "The Role of Defect Interaction in Boundary Mobility and Cation Diffusivity of CeO_2," *J. Am. Ceram. Soc.*, **77** [9] 2289–97 (1994).

[2]P.-L. Chen and I-W. Chen, "Grain Boundary Mobility in Y_2O_3: Defect Mechanism and Dopant Effects," *J. Am. Ceram. Soc.*, **79** [7] 1801–809 (1996).

[3]A. S. Nowick, D. Y. Wang, D. S. Park, and J. Griffith, "Oxygen-Ion Conductivity and Defect Structure of CeO_2"; pp. 673–81 in *Fast Ion Transport in Solids*. Edited by P. Vashishta, J. N. Mundy, and G. K. Shenoy. Elsevier North Holland, Amsterdam, Netherlands, 1979.

[4]R. Gerhardt-Anderson and A. S. Nowick, "Ionic Conductivity of CeO_2 with Trivalent Dopants of Different Ionic Radii," *Solid State Ionics*, **5**, 547–50 (1981).

[5]D. Y. Wang and A. S. Nowick, "Dielectric Relaxation from a Network of Charged Defects in Dilute CeO_2:Y_2O_3 Solid Solutions," *Solid State Ionics*, **5**, 551–54 (1981).

[6]I. K. Naik, "Electrical Properties, Nonstoichiometry and Defect Structures of Pure and Niobium Pentoxide-Doped Cerium Dioxide"; Ph.D. thesis. University of Michigan, Ann Arbor, MI, 1976.

[7]R. V. Blumenthal and R. K. Sharma, "Electronic Conductivity in Nonstoichiometric Cerium Dioxide," *J. Solid State Chem.*, **13**, 360–64 (1975).

[8]R. J. Panlener, R. N. Blumenthal, and J. E. Garnier, "A Thermodynamic Study of Nonstoichiometric Cerium Dioxide," *J. Phys. Chem. Solids*, **36**, 1213–22 (1975).

[9]O. T. Sorensen, "Thermodynamic Studies of the Phase Relationships of Nonstoichiometric Cerium Oxides at Higher Temperatures," *J. Solid State Chem.*, **18**, 217–33 (1976).

[10]H. Matzke, "Lattice Disorder and Metal Self-Diffusion in Nonstoichiometric UO_2 and (U,Pu)O_2," *J. Phys. (Paris) Suppl.*, **34** [11–12] C9-317–25 (1973).

[11]P.-L. Chen and I-W. Chen, "Reactive Cerium(IV) Oxide Powders by the Homogeneous Precipitation Method," *J. Am. Ceram. Soc.*, **76** [6] 1577–83 (1993).

[12]R. D. Shannon, "Revised Effective Ionic Radii and Systematic Studies of Interatomic Distances, Halides and Chalcogenides," *Acta Crystallogr.*, **A32**, 756 (1976).

[13]T. H. Etsell and S. N. Flengas, "The Electrical Properties of Solid Oxide Electrolytes," *Chem. Rev.*, **70** [3] 339–76 (1970).

[14]E. K. Keler, N. A. Godina, and A. M. Kalinins, "Reaction of Cerium Dioxide with Oxides of Alkaline-Earth Metals," *Zh. Neorg. Khim.*, **1** [11] 2556–60 (1956).

[15]H. H. Moebius, H. Witzmann, and F. Zimmer, "Rontgenographische Untersuchungen an Fluorite Phasen in den System des Scandium Oxides mit Zirkon-, Cer-, und Thorium Dioxide," *Z. Chem.*, **4**, 194–95 (1964).

[16]J. D. McDullough and J. D. Btitton, "X-ray Studies of Rare Earth Oxide System: II, The Oxide Systems Ce^{IV}–Sm^{III}, Ce^{IV}–Gd^{III}, Ce^{IV}–Y^{III}, Pr^{IV}–Y^{III}, and Pr^{IV}–Y^{III}," *J. Am. Ceram. Soc.*, **74**, 5225–27 (1952).

[17]E. Tani, M. Yoshimura, and S. Somiya, "Revised Phase Diagram of the System ZrO_2–CeO_2 Below 1400°C," *J. Am. Ceram. Soc.*, **66** [7] 506–10 (1983).

[18]R. L. Fullman, "Measurement of Particle Size in Opaque Bodies," *Trans. AIME*, **1970** [3] 447–52 (1953).

[19]J. E. Burke and D. Turnbull, "Recrystallization and Grain Growth in Metals," *Prog. Met. Phys.*, **3**, 220 (1952).

[20]I. K. Naik and T. Y. Tien, "Small-Polaron Mobility in Nonstoichiometric Cerium Dioxide," *J. Phys. Chem. Solids*, **38** [3] 311–15 (1978).

[21]M. H. Rand and T. L. Markin, "Some Thermodynamic Aspects of (U,Pu)O_2 Solid Solutions and Their Use as Nuclear Fuels"; pp. 637–50 in *Thermodynamics of Nuclear Materials*. International Atomic Energy Agency, Vienna, 1967.

[22]K. Z. Fung, A. V. Virkar, and D. L. Drobeck, "Massive Transformation in the Y_2O_3–Bi_2O_3 System," *J. Am. Ceram. Soc.*, **77** [6] 1638–48 (1994).

[23]S. L. Hwang and I-W. Chen, "Grain Size Control of Tetragonal Zirconia Polycrystals Using the Space Charge Concept," *J. Am. Ceram. Soc.*, **73** [11] 3269–77 (1990).

[24]R. J. Panlenar, R. N. Blumenthal, and J. E. Garnier, "A Thermodynamic Study of Nonstoichiometric Cerium Dixoide," *J. Phys. Chem. Solids*, **36** [11] 1213–22 (1975).

[25]H. Matzke, "Lattice Defects and Irradiation Damage in ThO_2, UO_2, and (U,Pu)O_2"; pp. 801–31 in *Plutonium 1975 and Other Actinides*. Edited by H. Blank and R. Lindner. North-Holland Publishing Co., Amsterdam, Netherlands, 1976.

[26]P. Li, I-W. Chen, J. E. Penner-Hahn, and T. Y. Tien, "X-ray Absorption Studies of Ceria with Trivalent Dopants," *J. Am. Ceram. Soc.*, **74** [5] 958–67 (1991).

[27]P. Li, I-W. Chen, and J. E. Penner-Hahn, "Effect of Dopants in Zirconia Stabilization—An X-ray Absorption Study: III, Charge-Compensating Dopants," *J. Am. Ceram. Soc.*, **77** [5] 1289–95 (1994).

[28]M. J. L. Sangster and A. M. Stoneham, "Calculations of Off-Centre Displacements of Divalent Substitutional Ions in CaO, SrO and BaO from Model Potentials," *Philos. Mag. B*, **43** [4] 597–608 (1981).

[29]A. N. Cormack, C. R. A. Catlow, and A. S. Nowick, "Theoretical Studies of Off-Centre Sc^{3+} Impurities in CeO_2," *J. Phys. Chem. Solids*, **50**, 177–81 (1989). □